A Comparison of Thruster Implementation Strategies for a Deep Space Nanosatellite

Matt Nehrenz*and Matt Sorgenfrei†

Attitude control for very small spacecraft, commonly referred to as nanosatellites or CubeSats, has traditionally been carried out using reaction wheels and magnetic torquers as the primary actuators. However, as these spacecraft begin to be considered for a broader range of scientific applications, including some beyond low Earth orbit, it has become necessary to also consider thruster systems for actuation. In recent years a number of thruster designs that conform to the mass, volume, and power constraints of nanosatellites have become commercially available, including cold gas systems, pulsed plasma thrusters (PPTs), and micro-electrospray propulsion (MEP) systems. The challenge now facing the nanosatellite community is to determine which thruster solutions are appropriate for a particular application, and what the best method of control might be. This paper will compare the implementation of a cold gas system with that of an MEP or PPT system for an upcoming nanosatellite mission using a previously reported saturation-restricted control law. Results are presented for this controller both with and without a fuel-optimal thruster allocation scheme, and an assessment on incorporating these technologies in an upcoming NASA mission is offered.

I.   Introduction

Attitude control for very small spacecraft has traditionally been undertaken using reaction wheels and magnetic torque coils or rods. Reaction wheels provide quick, comparatively accurate reorientation capabilities, while magnetic torquers can be used for slower, coarse control and for reducing momentum stored in the reaction wheels. However, as these spacecraft begin to be used for a wider range of tasks both in low Earth orbit (LEO) and beyond, the need for thrusters is becoming a more common requirement. Thrusters can provide attitude control with less jitter than poorly balanced reaction wheels (important for certain science applications [1]) and are required for momentum management of reaction wheels beyond low Earth orbit where magnetic torquers are no longer effective. As such, the small spacecraft community has begun to develop a wide range of thruster systems, including cold gas, pulsed plasma thrusters (PPTs), and micro-electrospray propulsion (MEP) solutions. This paper will present a comparison of implementing two such systems in a CubeSat-class spacecraft using a previously reported saturation-restricted control law [2].

For the purposes of this work, a CubeSat (also known as a nanosatellite) will refer to any spacecraft that weighs 14 kg or less. These spacecraft adhere to the CubeSat standard [3], whereby a 10 cm × 10 cm × 10 cm cube comprises one unit of volume, abbreviated as 1U. Traditional CubeSats are restricted to be no more than 3U in total volume, with an overall size of 10 cm × 10 cm × 30 cm. This volume constraint allows the spacecraft to be compatible with the various deployment mechanisms that are available, such as the Cal Poly P-POD [4]. NASA Ames has recently developed a new CubeSat deployer known as the Nanosatellite Launch Adapter System (NLAS), which is capable of deploying anywhere from six 1U spacecraft up to one 6U spacecraft. The NLAS dispenser achieved first flight in Fall of 2013, and has been manifested for use again in Fall of 2014 [5].

The application considered in this research is the upcoming BioSentinel mission, a 6U nanosatellite currently under development at NASA Ames. BioSentinel will launch as a secondary payload on the first flight of the Space Launch System (SLS), currently scheduled to occur in December of 2017. BioSentinel

---

*Matt Nehrenz is an Aerospace Engineer for Emergent Space Technologies in the Mission Design Division at NASA Ames Research Center, Moffett Field, CA 94035

†Matt Sorgenfrei is a Research Engineer for Stinger Ghaffarian Technologies in the Intelligent Systems Division at NASA Ames Research Center, Moffett Field, CA 94035

American Institute of Aeronautics and Astronautics

will likely be placed into an Earth-trailing, heliocentric orbit after tipping off from the second stage of SLS, after the rocket has placed the Orion Multi-Purpose Crew Vehicle on a trans-lunar injection trajectory. The science objective of BioSentinel is to study the impact of the deep space radiation environment on genetically modified yeast cells, building upon past NASA Ames space biology missions, such as the 3U PharmaSat spacecraft [6]. While the science payload itself does not impose severe attitude pointing requirements, it will be necessary to detumble the spacecraft after tip-off, and to also point a patch antenna back towards the Earth. These objectives could be achieved using reaction wheels and torque coils in a nanosatellite operating in LEO, but thrusters will be required for BioSentinel.

Very few nanosatellites have implemented propulsion systems on orbit, and those systems have generally been used only for translational maneuvers [7]. This work will consider the relative merits of integrating a cold gas thruster system [8] as compared to an MEP system [9] for attitude maintenance applications, with specific attention paid to the detumble maneuver. Detumble is affected using a controller that has previously been applied to saturation-restricted nanosatellite attitude control [10]. The commanded control torque is allocated to the available thrusters using two different approaches. In the first approach, the thruster pair which generates the largest control moment is always used to control a certain axis, while in the second approach a linear programming technique that utilizes the simplex method [11] is applied to allocate thruster firings in a fuel-optimal sense. An assessment of the two propulsion systems is made considering control authority, ease of integration into the candidate spacecraft, and the amount of fuel required to perform the detumble maneuver.

The reminder of this paper is organized as follows. First, the rotational dynamics of the 6U spacecraft under consideration is briefly reviewed, and the selected control law is presented. Next, the two different thruster geometries are introduced, and the methodologies for allocating thruster forces are presented. Simulation results are then presented for a detumble maneuver using both thruster designs, followed by a discussion of these results. The paper ends with some conclusions and recommendations for future research.

II.   Nanosatellite Dynamics and Control

II.A.   Nanosatellite Dynamics

For the heliocentric orbit currently being considered for BioSentinel, the rotational dynamics of the spacecraft will only be perturbed by a solar radiation pressure torque [12]. The equations of motion for the rotation of the spacecraft are given by Euler's equation [13] as

$$J\dot{\omega} + \omega \times J\omega = \tau + \tau_{sp} \tag{1}$$

where J is the inertia tensor for the spacecraft, ω is the angular velocity of the spacecraft in a body-fixed reference frame, τ is the control torque and τ_{sp} is the solar radiation pressure (SRP) torque. The SRP torque is defined as [12]

$$\tau_{sp} = \sum_n \bar{r}_n \times [\frac{F_s}{c} \cdot (1+q) \cdot A_{s_n} \cos(i_n) \cdot {}^b\hat{s}] \tag{2}$$

Note that this torque is defined as the sum of $n = 6$ individual torques due to the fact that the effect of the solar wind differs depending on how those particles interact with a particular face of the spacecraft. While the reflectance was conservatively held constant at $q = 1$ for all six faces, the projected surface area A_s, angle of incidence i, and offset from the center of gravity to an assumed center of pressure $\bar{r}$ all will differ for each of the six sides of the CubeSat. The solar constant $F_s = 1367$ W/m^2 and speed of light $c = 3\times10^8$ m/s were also held constant for all six torque terms in (2).

Rotation matrices are used to describe the orientation of the spacecraft body frame with respect to an inertial reference frame. Rotation matrices (denoted R) are members of the special orthogonal group $SO(3)$, defined as [14]

$$SO(3) = \{R \in \mathbb{R}^{3x3} : R^T R = I = RR^T, \det(R) = 1\}$$

and the evolution of a given rotation matrix R in time is governed by the equation

$$\dot{R} = RS(\omega) \tag{3}$$

where $S(\omega)$ is the skew-symmetric operator that carries a 3x1 vector into a 3x3 matrix [14]:

$$S(\omega) = \begin{bmatrix} 0 & -\omega_3 & \omega_2 \\ \omega_3 & 0 & -\omega_1 \\ -\omega_2 & \omega_1 & 0 \end{bmatrix}$$

Equations (1) and (3) fully describe the rotational motion of a spacecraft in the aforementioned heliocentric orbit. We further parameterize this motion by introducing expressions for the error in attitude and angular velocity, denoted as Q and ω_e respectively

$$Q = R_d^T R \tag{4}$$

$$\omega_e = \omega - Q^T \omega_d \tag{5}$$

where R_d and ω_d are the desired spacecraft attitude and angular velocity, respectively. The rotational motion of the spacecraft (equations (1) and (3)), parameterized by the rotational and angular velocity error (equations (4) and (5)), is what we seek to control using the thruster systems considered in this work.

II.B. Candidate Control Law

There are two main objectives for the attitude control system. The first is to stabilize the spacecraft after tip-off from SLS, when the spacecraft has high initial angular velocity and arbitrary orientation with respect to a given reference frame. The second objective is to point a body-mounted patch antenna towards the Earth in order to facilitate communications. In addition to these two active control maneuvers, the spacecraft attitude determination and control system (ADCS) must also counteract the effects of the solar radiation pressure torque while pointing deployable solar panels at the sun (seen in Figure 1 below). Reaction wheels have been selected as a primary attitude control actuator, but preliminary analysis has shown that these wheels will saturate while attempting to detumble the spacecraft. As such, it is desireable to study the feasibility of implementing a thruster system to support attitude control operations and to unload the stored momentum in the wheels.
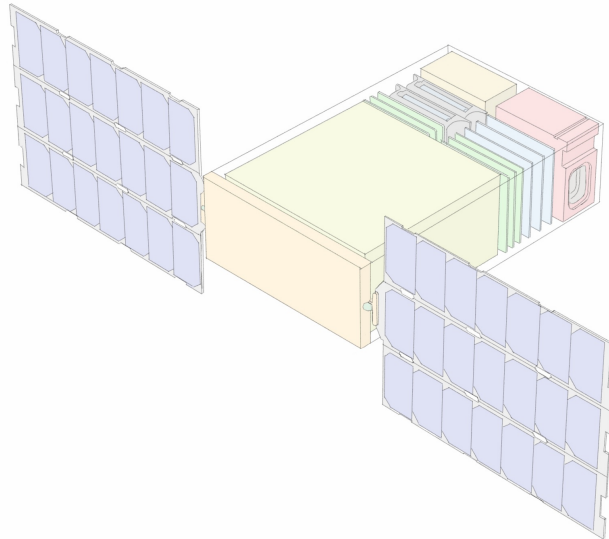

Figure 1 – Artist's depiction of the 6U BioSentinel spacecraft, shown with solar panels deployed

Due to the fairly severe mass, power, and volume restrictions that thruster systems for nanosatellites must adhere to, the maximum thrust available from any such system is comparatively low. As such, it is desireable to use a control law that can directly accomodate for saturation restrictions. The control law developed by Robinett, et al. in Reference [2] proposes a strategy in which the control torque applied to the system is determined by the maximum allowable value based on the saturation restrictions of available

American Institute of Aeronautics and Astronautics

actuators. Using this law, the control torque applied to the system is either the value determined from a proportional-derivative (PD) type controller (referred to as τ_{us}), or is a value corresponding to the maximum allowable control torque:

$$\tau_i = \begin{cases} \tau_{us_i} & \text{for} |\tau_{us_i}| \leq \tau_{max_i} \\ \tau_{max_i} \cdot \text{sgn}(\tau_{us_i}) & \text{for} |\tau_{us_i}| > \tau_{max_i} \end{cases} \tag{6}$$

where

$$\tau_{us} = J(Q\dot{\omega}_d - S(\omega_d)Q\omega_d) + S(\omega)J\omega - k\sigma - K_d\omega_e \tag{7}$$

The unsaturated commanded control torque τ_{us} uses scalar proportional gain k acting on the modified Rodrigues parameter (MRP) vector σ, and a diagonal 3×1 matrix derivative gain K_d acting on the angular velocity error ω_e. The MRP vector is defined in terms of the principal angle and the principal axis of rotational error using Euler's theorem on rotations [14]. Referencing Equation (6), the controller first determines whether or not the control torque calculated from Equation (7) is less than the maximum allowable control torque about each axis (e.g. for $i = 1 : 3$). If the control torque commanded by (7) does not exceed this value then that control torque is applied to each body axis. However, if the saturation limit is exceeded, then the saturation limit is instead applied, with the sense of that torque corresponding to the sense of the requested torque value. The reader is directed to [2] for a full treatment on the stability of this controller.

III. Thruster Implementation

The objective of the BioSentinel mission is to study the impact of the deep space radiation environment on genetically engineered yeast cells. These cells are dehydrated prior to launch, and then are rehydrated and kept alive in deep space using a microfluidics system and heaters. This payload requires approximately 4U (10cm × 20cm × 20cm) of volume, resulting in approximately 2U of volume remaining for all spacecraft bus subsystems (shown in the rear of the spacecraft in Figure 1). Due to the extreme volume limitations, it is anticipated that the thruster system will only be allowed to occupy approximately 0.5U of volume, plus some additional space for thruster nozzles. As can be seen in Figures 2 and 3, the nature of the thruster system used dramatically impacts where the thrust is actually imparted on the vehicle.

For a cold gas system that requires a more monolithic design, it is likely that the thrusters will be placed along the centerline of the spacecraft. Candidate cold gas systems [8] use four thrusters canted at 45° from the centerline, allowing for rotational control about all three body axes, as well as pure translation along the z-axis of the spacecraft (see Figure 2). CubeSat-class PPT and MEP systems typically make use of 2-3 electronics cards, and allow the user to separately place the thruster units themselves in different locations throughout the spacecraft. As seen in Figure 3, the initial approach considered for BioSentinel is to place a total of twelve thruster modules throughout the spacecraft, with three each located in each of the rear corners of the bus. Both of the thruster geometries allow for full attitude control while not violating the 4U volume allocated for the science payload. Certain thruster firings will not result in pure rotation–a translational component will be imparted on the spacecraft–but this is acceptable for the operational requirements of the BioSentinel mission. It is worth noting that due to uncertainty in the initial conditions of BioSentinel after tip-off from SLS, it is desireable to be able to impart a pure translational thrust, in the event that a ΔV manuever is required to keep the spacecraft in its ideal orbit.

For each of the thruster systems under consideration, the first approach taken was to determine the maximum possible control torque available about each body axis based on the orientation of the thrusters with respect to those axes. The thrusters of the cold gas system can produce a maximum thrust of 40 mN, while the thrusters of the MEP system can produce a maximum of 100 μN. This maximum thrust value, multiplied by the moment arm from the center of gravity to the line of action of the thrust, determines the saturation limits used in Equation (6). It was assumed that any value from zero to the maximum thrust value could be commanded by the system. Additionally, in the event that multiple thruster pairs could impart a control torque (as is the case in Figure 3), the pair which resulted in the larger torque was used.

Using the same rules for how the maximum control torque could be generated, the second approach taken was to minimize the fuel consumed by the thrusters, following the methodology in Reference [15]. Specifically, one can seek to minimize the function
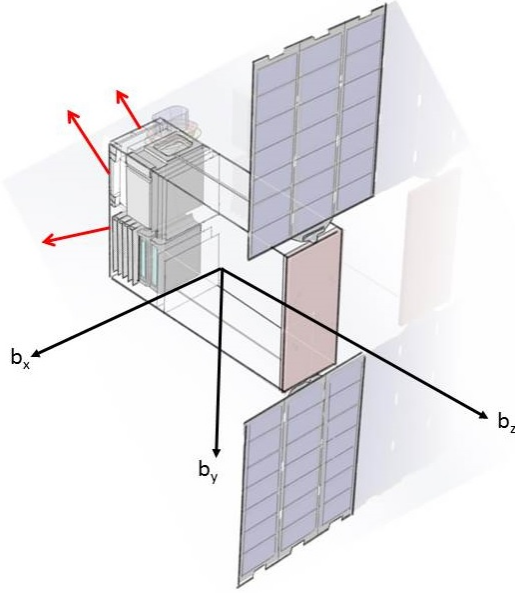
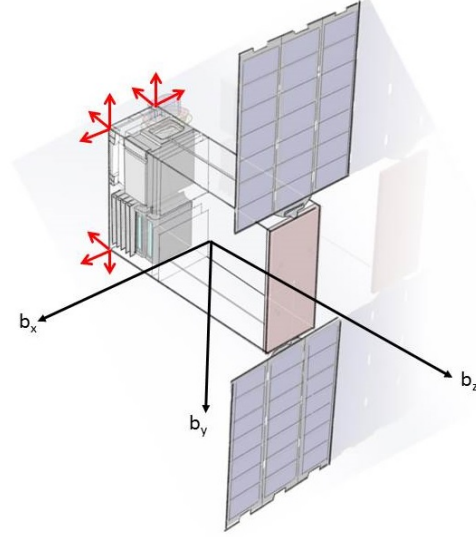Figure 2 – Thrust vectors enabled by a four-nozzle cold gas thruster system

Figure 3 – Thrust vectors enabled by a electrical thruster system in which twelve thrusters can be placed individually

$$J = \sum_{i=1}^{n} x_i \tag{8}$$

where n is the number of thrusters available in the system. This minimization is subject to the linear constraints

$$\begin{bmatrix} \bar{F}_c \\ \bar{T}_c \end{bmatrix} = \begin{bmatrix} H_f \\ H_t \end{bmatrix} \bar{x} \tag{9}$$

and

$$0 \le x_i \le x_{max}, \text{ for } i = 1, ..., n \tag{10}$$

The control forces F_c and the control torques $\bar{T}_c$ seen in Equation (9) are each 3×1 column vectors, where $\bar{F}_c = \begin{bmatrix} F_x & F_y & F_z \end{bmatrix}^T$ and $\bar{T}_c = \begin{bmatrix} T_x & T_y & T_z \end{bmatrix}^T$. These forces and torques are are imparted by virtue of a $6 \times n$ distribution matrix H, whose top half describes the geometry of how forces are imparted (H_f) and whose bottom describes how torques are imparted (H_t). The column vector $\bar{x}$ contains the thrust values themselves, which are non-zero and cannot exceed a known maximum value x_{max}, as defined in (10). Returning to Figure 2, given that there are four cold gas thrusters the distribution matrix for this system will be 6×4. Each of the trusters is canted at $45°$, and none of the trusters act in the x direction, resulting in the first row of zeros in Equation (11) and a multiplier of 0.707 ($\frac{\sqrt{2}}{2}$) everywhere else. The control torques are a function of the moment arm from the center of gravity to the line of action of each thruster, defined by the vector $\bar{rg} = \begin{bmatrix} rg_x & rg_y & rg_z \end{bmatrix}^T$. The sense of all of the terms in (11) is derived from the basic geometry of the spacecraft, and whether or not the resulting force or torque is positive or negative.

$$H = \begin{bmatrix} 0 & 0 & 0 & 0 \\ -0.707 & -0.707 & 0.707 & 0.707 \\ -0.707 & -0.707 & -0.707 & -0.707 \\ 0.707(rg_z - rg_y) & 0.707(rg_z - rg_y) & 0.707(rg_y - rg_z) & 0.707(rg_y - rg_z) \\ 0.707rg_x & -0.707rg_x & -0.707rg_x & 0.707rg_x \\ -0.707rg_x & 0.707rg_x & -0.707rg_x & 0.707rg_x \end{bmatrix} \tag{11}$$

American Institute of Aeronautics and Astronautics

The distribution matrix H is generated in a similar manner for the MEP system. In this case there are 12 thrusters, resulting in 6×12 matrix. Since there are thrusters aligned with each body axis the force portion of the matrix H_f is populated with either 1's or 0's, in that a given thruster either can or cannot contribute thrust in that direction. Once again the control torques are a function of a moment arm from the center of gravity to the thruster locations, referred to as $r\bar{m}$. Note that in this case there are four vectors, $r\bar{m}_1$ to $r\bar{m}_4$, one each for each cluster of thruster modules in each corner of the spacecraft. Again, the sense of these terms is derived from the spacecraft geometry, in this case evidenced by Figure 3.

$$
H = \begin{bmatrix}
1 & 0 & 0 & -1 & 0 & 0 & -1 & 0 & 0 & 1 & 0 & 0 \\
0 & 0 & 1 & 0 & 0 & 1 & 0 & 0 & -1 & 0 & 0 & -1 \\
0 & 1 & 0 & 0 & 1 & 1 & 0 & 1 & 0 & 0 & 1 & 0 \\
0 & -rm_{1y} & rm_{1z} & 0 & -rm_{2y} & rm_{2z} & 0 & rm_{3y} & -rm_{3z} & 0 & rm_{4y} & -rm_{4z} \\
-rm_{1z} & rm_{1x} & 0 & rm_{2z} & -rm_{2x} & 0 & rm_{3z} & -rm_{3x} & 0 & -rm_{4z} & r_{4x} & 0 \\
rm_{1y} & 0 & -rm_{1x} & -rm_{2y} & 0 & rm_{2x} & rm_{3y} & 0 & -rm_{3x} & -rm_{4y} & 0 & rm_{4x}
\end{bmatrix}
$$
(12)

While the linear constraints defined by Equations (11) and (12) don't impact the control torque that is imparted upon the spacecraft, they will play a role in optimizing which thrusters are fired when, which should result in an overall fuel savings for the detumble manuever. This will be investigated in the next section.

IV.   Simulation Results

Each of the thruster systems described previously are used to detumble the BioSentinel spacecraft. The current design of the system calls for the spacecraft to be 14 kg in mass, with this mass homogenously distributed throughout the available volume. This results in an inertia tensor of $J = \mathrm{diag}(\begin{bmatrix} 0.218 & 0.166 & 0.082 \end{bmatrix})$. It is assumed that the spacecraft will have an initial angular velocity of $5°$/sec about each body axis, and it is the objective of the control law of Equation (6) to drive this angular velocity to zero. The first system tested is the cold gas system whose thrust vectors are depicted in Figure 2. The time history of the spacecraft angular velocity and the commanded control torques are plotted in Figure 4.
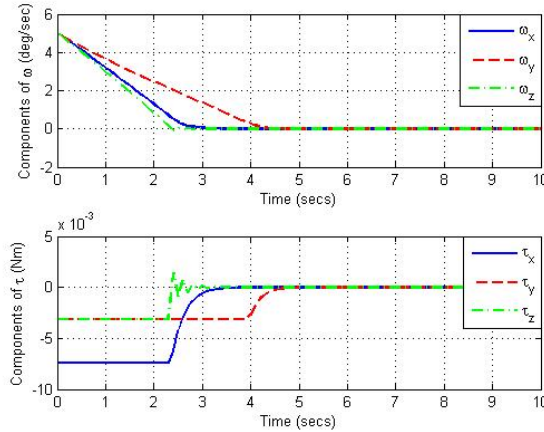

Figure 4 – Components of spacecraft angular velocity (top plot) and commanded control torque (bottom plot) using the cold gas system.

The comparatively high control authority of cold gas system results in a very quick detumble maneuver, and the motion of the spacecraft is really not effected by the action of the solar radiation pressure disturbance. This is evidenced in Figure 5, where the components of the control torque are quickly stabilized. The elements of the unit vector to the sun resolved in the body frame (s_B) are also included in Figure 5 to help the reader visualize the orientation of the spacecraft with respect to the heliocentric frame. The detumble maneuver drives the spacecraft to zero angular velocity with respect to an intermediate orbit frame, but at Earth

American Institute of Aeronautics and Astronautics

distances from the sun this frame only rotates with respect to the inertial sun frame one degree per day.
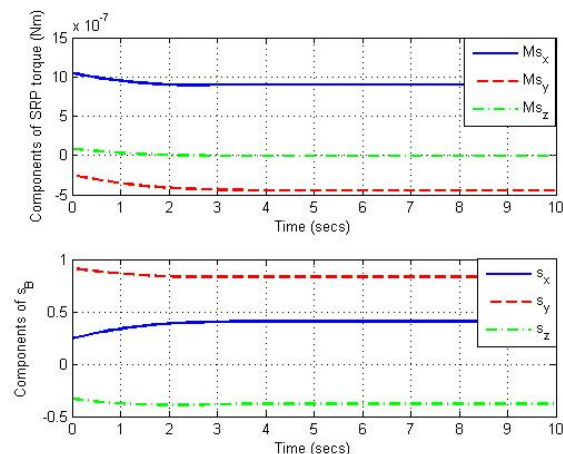

Figure 5 – Components of the solar radiation pressure torque (top plot) and elements of the solar unit vector during the detumble manuever.

The detumble maneuver is more challenging for the MEP system, whose control authority is much less than that of the cold gas system. While the cold gas system was able to detumble the spacecraft in less than 10 seconds, it takes the MEP system close to 1200 seconds to perform the same control task.
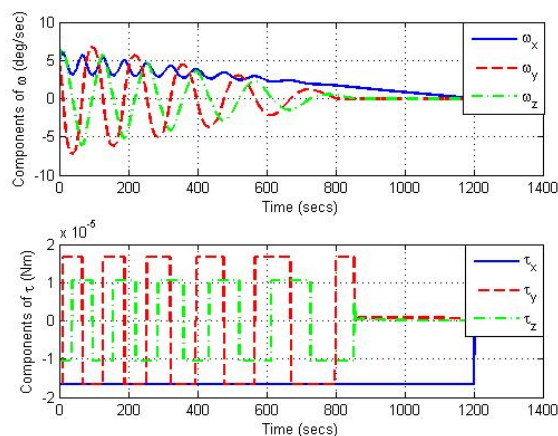

Figure 6 – Components of spacecraft angular velocity (top plot) and commanded control torque (bottom plot) using the micro-electrospray propulsion system.

Unsurprisingly, the impact of the solar radiation pressure torque during detumble is much more pronounced when using the MEP system. The control torque that can be imparted by the MEP thrusters is only one order of magnitude higher than the components of the SRP torque (10^{-5} Nm as opposed to 10^{-6} Nm), and as a consequence it takes much longer for the controller to be able to reject the effects of this disturbance.

An important consideration when selecting which thruster system to use for the BioSentinel spacecraft is how much propellant is consumed by each system when performing the detumble maneuver. The baseline mission life for BioSentinel is twelve months, with a stretch goal of 18 months, and the propulsion system must be capable of supporting operations throughout that entire lifetime. This long mission life, combined with the severe volume limitations within the spacecraft, make propellant efficiency very important. The amount of propellant consumed by each system can be calculated using

$$\dot{m} = \frac{F}{I_{sp}g} \tag{13}$$

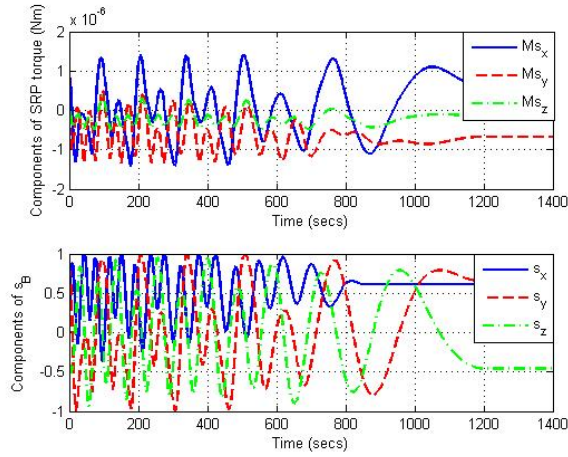American Institute of Aeronautics and Astronautics

Figure 7 – Components of the solar radiation pressure torque (top plot) and elements of the solar unit vector during the detumble manuever.

where F is the thruster force, I_{sp} is the specific impulse, and g is the gravitational constant on Earth. The cold gas system under consideration has an I_{sp} of 60 seconds, while the MEP system has an I_{sp} of 1500 seconds. The amount of propellant consumed by each system both with and without the fuel optimization approach described in the preceding section is given in Table 1

Table 1 – Propellant mass consumed for the detumble maneuver with and without the fuel optimization strategy

System	Mass (g)	Optimized Mass (g)
Cold Gas	1.3	0.67
MEP	0.01428	0.01420

It is interesting to observe that the fuel savings achieved using the optimization process described in Section III only yields about 0.6% savings for the MEP system, as compared to a full 94% savings for the cold gas system. The optimization scheme is clearly providing a savings in the amount of fuel consumed in both cases, however the drastic decrease in this savings for the MEP system is largely due to the configuration of the thruster modules. Referring back to Figure 3, there are thruster pairs that are capable of affecting a control torque about each body-fixed axis. Depending on which thruster pair is used a different moment arm will cause the control torque, resulting in different levels of control authority. As such, the optimization scheme can select which thruster pair to fire in order to minimize the amount of fuel consumed. However, the spacecraft designer can analytically determine which thrusters to actuate for a given torque direction based on largest moment arm. The control torque/thruster pair relationship is not as readily apparent for the four cold gas thrusters because each thruster contributes torque about all three axes, and the optimization scheme is able to contribute a substantial savings in fuel.

V. Discussion

A first appraisal of the results in the preceding section seems to indicate that either system could be sufficient for the ADCS needs of the BioSentinel mission. The MEP system takes substantially longer to detumble the spacecraft, but the amount of time in which detumble must occur (driven by available battery life) is on the scale of 5-6 hours, making a 10 minute detumble operation acceptable. Not considered in this work is the impact of managing the momentum of the reaction wheels, which will saturate periodically due to the effects of the SRP torque. Over the twelve month nominal mission life the need to desaturate the reaction wheels will become the driving design factor for the amount of fuel that must be stored, which could ultimately result in an MEP system being selected for use. The monolithic fuel tank associated with cold gas systems might become too much of a volume penalty, given the fact that all bus operations must be

contained within 2U of volume. If it is possible to place smaller amounts of fuel in multiple discrete locations (as enabled by MEP or PPT designs) then such a system may prove more viable, even with the significantly smaller control authority.

One interesting consequence of the thruster layouts considered in Section III is that there are certain axes about which the commanded control torque will result in a translation being imparted upon the spacecraft. For spacecraft applications in which it is unacceptable to translate as a result of an attitude control maneuver the commanded force vector $\bar{F}_c$ can be set to zero in the constraint equation (9). This will result in thruster firings that negate any translational motion while still performing the necessary rotation. For the detumble and momentum management tasks of the BioSentinel thruster system a small amount of tranlsational motion is acceptable. Thus, for these attitude control maneuvers, it is possible to structure the thruster allocation constraint as $\bar{T}_c = H_t \bar{x}$, which removes any consideration of translational motion. This is the approach that was taken to generate the fuel consumption values in the second column of Table 1. However, it is likely that BioSentinel will need to perform one or more orbital during its mission life, and for these phases of operation a full 6 row constraint matrix H will be used.

It is important to acknowledge that a simplification undertaken in this research was to neglect the impacts of noise in the system. It was assumed that the controller had perfect knowledge of the spacecraft state, and that "clean" torques could be commanded by each of the thruster systems. While state estimation approaches would likely help to reduce the majority of chatter that could impact the thrusters, it is unlikely that either thruster system would be able to produce the torque curves presented in the previous section. For both the cold gas and MEP technologies a certain amount of pulse width modulation will be required to obtain the desired thrust level, which will result in a noiser response than what has been presented here. It is unlikely that any system noise would drastically alter the comparison between cold gas and MEP technologies, but MEP and PPT systems often make use of high voltage wiring, which could exacerbate any electronic noise that the attitude determination system is combating. Ultimately the biggest impact would be on the overall amount of fuel consumed, which is already a driving consideration in the final selection of a propulsion system for BioSentinel.

The authors are currently developing an additional aspect of this research which takes into account fuel optimization not as a function of an overall monolithic fuel tank, but for a configuration in which each thruster contains its own fuel resevoir. Each thruster head in an MEP or PPT system often has its own fuel supply, and simulation results from this work have shown that certain thrusters are used more often due to varying moment arms and commanded torques. As such, it would be valuable to augment the existing linear programming approach to consider the amount of fuel consumed by each individual thruster. If the existing optimization results in certain thrusters being fired more regularly than others, then it is possible that later into the BioSentinel mission life those thrusters will be depleted of fuel. In addition to augmenting the linear programming problem, attention can be directed to supplying thrusters that have been shown in simulation to be used more regularly with a larger fuel reserve. The inclusion of additional constraints into the existing optimization approach is in progress, and will be included in the final draft of this paper should it be accepted for presentation at SciTech 2015.

VI.   Conclusion

This paper presents a comparison of two different approaches for implementing thruster systems in a CubeSat-class spacecraft that will operate in deep space. While the high control authority of the cold gas system makes it ideal for the control operations that must be carred out on orbit, its monolithic design and larger volume will make it challenging to integrate it into the final spacecraft. In contrast, the MEP system offers much lower control, but can be integrated into multiple discrete locations throughout the spacecraft by virtue of its modular design. Both systems are capable of performing the detumble maneuver in an acceptable amount of time, although the lower control authority of the MEP system is evidenced in how much longer it takes to stabilize the solar radiation pressure torque during detumble. This work did not take into consideration the execution of any translational maneuvers, and it is possible that the need to make a quick, impulsive burn in order to change the trajectory of BioSentinel could cause the spacecraft designers to favor a cold gas system in the final formulation of the mission.

References

[1] Bayard, D., "State-Space Approach to Computing Spacecraft Pointing Jitter," *Journal of Guidance, Control, and Dynamics*, Vol. 27, No. 3, 2004, pp. 426–433.

[2] Robinett, R., Parker, G., Schaub, H., and Junkins, J., "Lyapunov Optimal Saturated Control for Nonlinear Systems," Vol. 20, No. 6, 1997, pp. 1083–1088.

[3] Nugent, R., "The CubeSat: The Picosatellite Standard for Research and Education," *Proc. of AIAA Space Conference and Exhibit*, San Diego, California, September 2008.

[4] Puig-Suari, J. et al., "Development of the Standard CubeSat Deployer and a CubeSat Class Picosatellite," *Proc. of IEEE Aerospace Conference*, Big Sky, Montana, March 2001.

[5] Sorgenfrei, M., Nehrenz, M., and Shish, K., "Operational Considerations for a Swarm of CubeSat-Class Spacecraft," *Proc. of the AIAA SpaceOps Conference*, Pasadena, California, May 2014.

[6] Diaz-Aguado, M. et al., "Small Class-D Spacecraft Thermal Design, Test, and Analysis-PharmaSat Biological Experiment," *Proc. of IEEE Aerospace Conference*, Big Sky, Montana, March 2009.

[7] Mauthe, S., Pranajaya, F., and Zee, R., "The Design and Test of a Compact Propulsion System for CanX Nanosatellite Formation Flying," *Proc. of AIAA/USU Conference on Small Satellites*, Logan, Utah, August 2005.

[8] Arestie, S., Lightsey, E., and Hudson, B., "Development of a Modular, Cold Gas Propulsion System for Small Satellite Applications," *Journal of Spacecraft and Rockets*, Vol. 1, No. 2, 2012, pp. 63–74.

[9] Coffman, C., Perna, L., Li, H., and Lozano, P., "On the Manufacturing and Emission Characteristics of a Novel Borosilicate Electrospray Source," *Proc. of the 49th Joint Propulsion Conference*, San Jose, California, July 2013.

[10] Sorgenfrei, M. and Joshi, S., "Reconfigurable Spacecraft Controller Design via Location-Scheduled Control," Vol. 34, No. 5, 2011, pp. 164–173.

[11] Wie, B., *Space Vehicle Dynamics and Control*, AIAA, 2nd ed., 2005, pp. 450–457.

[12] (ed.), J. W., *Space Mission Analysis and Design*, D. Riedel Publishing Co., 1st ed., 1978, pp. 410–412.

[13] Kane, T., Likins, P., and Levinson, D., *Spacecraft Dynamics*, McGraw-Hill, 1st ed., 1983, pp. 120–122.

[14] Bullo, F. and Lewis, A., *Geometric Control of Mechanical Systems*, Springer, 2005, pp. 300–320.

[15] Curti, F., Romano, M., and Bevilacqua, R., "Lyapunov-Based Thrusters' Selection for Spacecraft Control: Analysis and Experimentation," *Journal of Guidance, Control, and Dynamics*, Vol. 33, No. 4, 2010, pp. 1143–1160.